NJC

Accepted Manuscript

This is an *Accepted Manuscript*, which has been through the Royal Society of Chemistry peer review process and has been accepted for publication.

Accepted Manuscripts are published online shortly after acceptance, before technical editing, formatting and proof reading. Using this free service, authors can make their results available to the community, in citable form, before we publish the edited article. We will replace this *Accepted Manuscript* with the edited and formatted *Advance Article* as soon as it is available.

You can find more information about *Accepted Manuscripts* in the Information for Authors.

Please note that technical editing may introduce minor changes to the text and/or graphics, which may alter content. The journal's standard Terms & Conditions and the Ethical guidelines still apply. In no event shall the Royal Society of Chemistry be held responsible for any errors or omissions in this *Accepted Manuscript* or any consequences arising from the use of any information it contains.

ROYAL SOCIETY OF CHEMISTRY

www.rsc.org/njc

Synthesis of Shape-Controlled NiO/Graphene Nanocomposites with Enhanced Supercapacitive Properties

Xiaomiao Feng,*[a1] Jinhua Zhou,[a1] Linlin Wang, [1] Yi Li, [1] Zhendong Huang, [1] Shufen Chen, [1] Yanwen Ma,* [1] Lianhui Wang, [1] and Xiaohong Yan[2]

[1] Key Laboratory for Organic Electronics and Information Displays & Institute of Advanced Materials, National Jiangsu Syngerstic Innovation Center for Advanced Materials (SICAM);

[2] College of Electronic Science and Engineering,

Nanjing University of Posts & Telecommunications, 9 Wenyuan Road, Nanjing 210023, China

* Corresponding authors.

E-mail addresses: iamxmfeng@njupt.edu.cn, iamywma@njupt.edu.cn

[a] These authors contributed equally to this work.

Abstract: Flowerlike and polyhedral NiO/graphene nanocomposites have been successfully synthesized by a facile hydrothermal method. The formation mechanism of the two nanocomposites with different morphologies has been studied. The resulting products are characterized by scanning electron microscopy (SEM), transmission electron microscope (TEM), X-ray diffraction (XRD), Fourier transform infrared spectroscopy (FT-IR), X-ray photoelectron spectroscopic analysis (XPS), thermogravimetry (TG), and Brunauer-Emmett-Teller (BET). The prepared NiO/graphene nanocomposites with different shapes can be used for supercapacitor electrode materials. Through electrochemical tests, the flowerlike NiO/graphene composite shows higher specific capacitance than that of the polyhedral one with a specific capacitance as high as 500 F/g at a scan rate of 5 mV/s while the polyhedral NiO/graphene composite delivers better long-term cycle stability with 84% specific capacitance remaining after 3000 cycles in 1 M KOH electrolyte.

Introduction

With the rapid development of the global economy, the depletion of fossil fuels and increasing environmental pollution, there is an urgent need for efficient, clean, and sustainable sources of energy, as well as new technologies associated with energy conversion and storage.[1] In many application areas, some of the most effective and practical technologies for electrochemical energy conversion and storage are batteries and electrochemical capacitors.[2] Batteries can keep devices work throughout the day,

but they take hours to recharge when they run down. For rapid power delivery and recharging (i.e., high power density), electrochemical capacitors are good candidates. Electrochemical capacitors, also called supercapacitors, can be divided into two classes based on the different energy storage mechanisms: electrochemical double-layer capacitors (EDLCs) which store energy by the adsorption of ions and pseudo-capacitors that store energy through fast surface redox reactions.[3] EDLCs normally use carbon-based materials due to its outstanding electrochemical stability, good conductivity, low cost, and availability in various different forms.[4] Metal oxides and conducting polymers are widely used as electrode materials for pseudocapacitors.[5] As the charge accumulation is purely electrostatic, the energy density of the EDLCs is limited by the available surface area of the electrode material.[6] Though the higher capacitance, the pseudo-capacitors delivered low power density, bad cycling stability, and poor rate capability (dramatic drop of specific capacitance with an increased scan rate) because of poor electrical conductivity.[7] For improving the properties of supercapacitors, the composites combined double layer capacitance with pseudo-capacitance are used widely in order to get superior performances.[8]

Graphene is a two-dimensional sheet of sp^2-hybridized conjugated carbon atoms with extended honeycomb network structure,[9, 10] due to its high electrical and thermal conductivities, good transparency, great mechanical strength, inherent flexibility, and huge specific surface area.[11] Thus, it is expected to be an ideal material for energy storage and conversion and also has attracted a great deal of attention in many other areas.[12-15] Recently, lots of investigations have been focused on the graphene-based composites for supercapacitors,[16-18] especially for graphene-transition metal oxide composites because they can combine the advantages of two components and offer special properties through the reinforcement or modification of each other.[19-21] To date, graphene-transition metal oxides composites, such as MnO_2/graphene,[22] SnO_2/graphene,[23] TiO_2/graphene,[24] Co_3O_4/graphene,[25] and Fe_3O_4/graphene[26], have been studied and expected to show improved capacitance owing to their enhanced

electronic conductivity and the unique nanostructure of graphene.

Among all the transition metal oxides, nickel oxide (NiO) appears to be a promising candidate applied in supercapacitors due to its high theoretical specific capacitance, large surface area, low cost, and environmentally friendly.[27] In the past few years, many synthetic techniques have been explored in the preparation of NiO with different morphologies and structures such as microspheres,[28-30] nanowalls,[31-33] nanopwires,[34] nanoplates,[35] and nanoflowers.[36, 37] However, NiO usually delivers poor rate capability and reversibility during the charge/discharge process due to its relatively poor electrical conductivity and low accessible surface areas. Therefore, many investigations were focused on combination NiO with conductive materials to improve the electrochemical performances, such as activated carbon[38], carbon nanotubes,[39] and graphene are the main candidates. Xing et al. reported a specific capacitance of 124 F/g at a current density of 0.1 A/g for a spherical mesoporous NiO.[40] Polyhedron shaped NiO exhibited a specific capacitance of 165 F/g at a scan rate of 5 mV/s.[41] Graphene porous NiO nanocomposite was synthesized by a facile hydrothermal route, delivering a specific capacitance of 429.7 at 0.2 A/g, reported by Jiang et al..[42] Monolayer graphene/NiO nanosheets based on self-assembly displayed a specific capacitance of 525 F/g at a current density of 0.2 A/g.[43]

In this report, flowerlike and polyhedral NiO/graphene composites were synthesized by a simple thermal treatment process, respectively. When Graphene oxide (GO) precursor handled with vacuum freeze-drying process, the as-prepared nanocomposite appeared a good-looking flowerlike structure. On the other operation that GO suspension was the substitute, the final corresponding composite presented a polyhedral structure. SEM results confirm NiO was anchored on the graphene sheets. The XPS spectrum demonstated NiO adhered to graphene through a C-O-Ni linkage. XRD, FT-IR, and TG were also used to investigate the structure and composition of NiO/graphene nanocomposites. The as-prepared NiO/graphene nanocomposites had been used for supercapacitor electrode materials. Through electrochemical tests, the flowerlike NiO/graphene nanocomposite showed higher specific capacitance than that

of the polyhedral one with a specific capacitance as high as 500 F/g at a scan rate of 5 mV/s while the polyhedral NiO/graphene composite delievers better long-term cycle stability with 84% specific capacitance remaining after 3000 cycles in 1 M KOH electrolyte.

2. Experimental

2.1 Chemicals

Natural graphite flake (about 325 mesh) was purchased from Alfa Aesar Chemical Reagent Co. Nickel(II) chloride hexahydrate ($NiCl_2{\cdot}6H_2O$), urea, acetylene black, polytetrafluorene ethylene (PTFE), potassium hydroxide (KOH), and ethanol were purchased from Shanghai Chemical Reagent Co. All reagents were analytical grade and used as received without further purification.

2.2 Preparation of different morphologies NiO/graphene composites

GO was prepared through the modified Hummer's method from natural flake graphite powder as described previously.[44] Part of the as-prepared GO suspension was dried by vacuum freeze-drying and the rest of GO suspension was used directly. Flowerlike graphene/NiO nanocomposites were synthesized by the following steps: 1.6(mmol) nickel (II) chloride hexahydrate ($NiCl_2{\cdot}6H_2O$) were added into freeze-drying GO sloution (90 mg freeze-drying GO were dispersed in 60 mL DI water) and kept vigorous stirring for 30 minutes at ambient temperature. Subsequently, 10 (mmol) urea dissolved in 10 mL water was added into the above solution drop by drop and kept magnetic stirring for 30 minutes. The resulted mixture was removed into a Teflon-Lined autoclave with a stainless-steel shell, maintained at 180 $^{\circ}$C for 2 h. Subsequently, the precipitate was separated and washed with distilled water and ethanol. Then, it was dried at 60 $^{\circ}$C under a vacuum overnight. The precursor obtained was further calcinated in flowing argon by heating at the rate of 10 $^{\circ}$C/min from room temperature to 400 $^{\circ}$C and maintained for 2 h to obtain the final composites. Meanwhile, the GO suspension containing the equal mass GO was used to synthesis the polyhedral NiO/graphene nanocomposites, and the other experimental conditions were same with the above. For a comparision, pure NiO and rGO were prepared by

the same process.

2.4 Characterization

The morphologies of nanocomposites were characterized by scanning electron microscopy (SEM, S-4800) and transmission electron microscope (TEM, JEOL-JEM-2100F at 100 kV). The structure of nanocomposites was investigated by means of X-ray diffraction patterns (XRD, Philip-X'Pert X-ray diffractometer). The composition of products was examined by Fourier transform infrared spectroscopy (FT-IR, a Bruker model VECTOR-22 Fourier transform spectrometer). The X-ray photoelectron spectroscopic analysis was obtained using ESCA-LAB MK II X-ray photoelectron spectrometer. Brunauer-Emmett-Teller (BET) specific surface areas were determined from nitrogen sorption isotherms that were obtained from a V-Sorb2800P analyzer at 77 K. The thermogravimetry (TG) measurements were carried out with a NETZSCH STA449C thermal analyzer. Electrochemical experiments were investigated by a CHI660C electrochemical workstation (Chenhua, Shanghai). The three-electrode cell consisted of a platinum wire as counter electrode and saturated calomel electrode (SCE) as reference electrode, respectively. The working electrode was prepared by mixing active material, acetylene black, and polyfluortetraethylene (PTFE) at a weight ratio of 70: 25: 5 and pasted onto graphite electrode. The average loading mass of mixed materials were about 10 mg on per extrode. The specific capacitance could be calculated from the cyclic voltammograms (CV) curves according to eqn 1[45]:

$$C_g = \frac{(\int I dv)}{(mVv)} \quad (1)$$

Where I is the response current, V is the potential range, υ is the scan rate, and m is the mass of the active material in the electrode. The specific capacitance was calculated from the galvanostatic charge/discharge curves using eqn 2[46]:

$$It \quad (2)$$

Where I represent the discharge current (A), Δt is the discharge time (s), m is the mass

of the active material in the electrode, and ΔV is the potential window .

3. Results and discussion

The NiO/graphene nanocomposites with different shapes were synthesized by a simple hydrothermal treatment process. When GO was handled with freeze-drying process, the obtained NiO appealed a good-looking flowerlike structure. While the as-prepared GO suspension without vacuum freeze-drying process was used, the final corresponding NiO showed a polyhedral structure. The pure NiO flowers expressed a flowerlike shape by lack of GO. Fig. 1A and 1B showed the SEM images of the flowerlike NiO/graphene nanocomposites. From Fig. 1A, we could see that the NiO/graphene nanocomposite had been successfully prepared after hydrothermal process and graphene acted as support material with NiO on it. (Fig S1). In the view of NiO at high magnification, as shown in Fig. 1B, it displayed a good-looking flower with an average size of 4 μm. The 3D flower-like architecture was formed from the primary nanosheets assembling by driving forces, such as crystal-face attraction, van der Waals forces, and hydrogen bonds.[47, 48] The images of polyhedral NiO/graphene nanocomposite were shown in Fig. 1C and 1D. In the two pictures, thin and crumpled graphene sheets could be seen and polyhedral NiO with an average size ranging from 50 nm to 70 nm anchored on graphene nanosheets uniformly. The flowerlike and polyhedral NiO/graphene nanocomposites were denoted as GN-f and GN-p, respectively. The presence of NiO effectively prevented the agglomeration and restacking of graphene and helped maintain their high active surface area, which was favorable to increase accessible reaction sites to enhance the supercapacitive properties.

The formation mechanism of the nanocomposites with different shapes could be described as follows: Firstly, when GO sheets solution was mixed with $NiCl_2$, Ni^{2+} ions could anchor onto the surface of GO and effectively bond with the oxygen-containing functional groups of GO through electrostatic attraction. Then, nickel ions, which were adsorbed on both side of graphene nanosheets, react with urea to produce basic nickel hydroxide depositing on graphene sheets. These nanoparticles

also prohibited the stacking of graphene sheets by van der Waals forces. After the hydrothermal process, GO was reduced to graphene. Finally, the precursor was heated at 400 °C in Ar for 2 h to obtain the final product of NiO/graphene nanocomposites. During the calcinations process, the basic nickel hydroxide was decomposed into nickel oxide[49]. Increased interlayer distance of GO sheets could be retained by vacuum freeze-drying, which benefitting to provide sufficient growth space. The reaction between Ni^{2+} ions and urea could be carried out completely because of the presence of sufficient growth space. At the first stage, nickel hydroxide nanosheets generated as the main morphology and then flowerlike nickel hydroxide would be formed by crystal-face attraction, van der Waals forces, and hydrogen bonds via previous nanosheets self-agglomerating.[50, 51] The flowerlike structure could be maintained in the next calcinations process. By comparison, GO suspension brought narrow interlayer distance, Ni^{2+} ions were wrapped between grpahene layers and could not get full access with urea, then nickel hydroxide crystal nucleus could not get sufficient space to grow. On the other hand, the increase of viscosity in the reaction system restricted the growth of nickel hydroxide particles in some directions when GO suspension was used.[52] The nickel hydroxide particles caused the exfoliation of lamellar GO. As a result, the smaller polyhedral NiO/graphene was obtained. As a result, the smaller polyhedral NiO/graphene was obtained.[41]

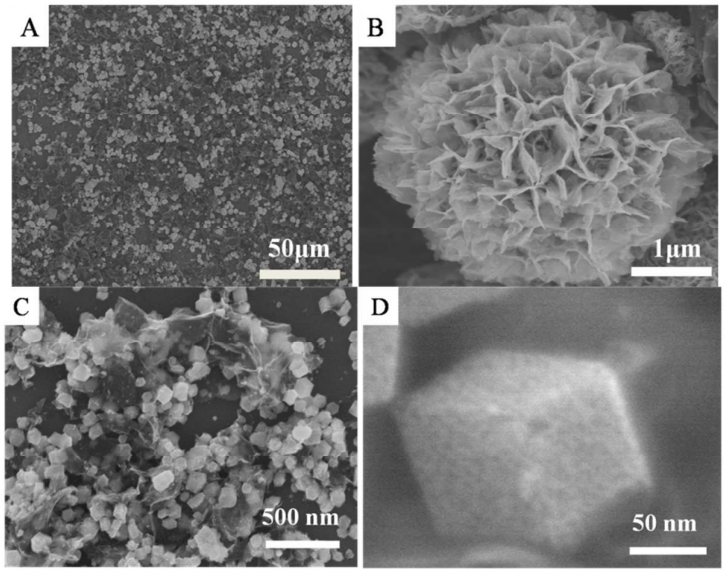

Fig. 1. SEM images of GN-f (A/B) and GN-p (C/D) with different magnifications.

Fig. 2 shows the XRD patterns of freeze-drying GO, pristine GO, GN-f, and GN-p. Obviously, the pristine GO shows a strong diffraction peak at around 10.7 · corresponding to the (001) reflection of the stacked GO sheets. For freeze-drying GO, the (001) diffraction peak has shifted to small angle (about 10.0 ·) and becomes much weaker than that of the pristine GO. The stronger (001) diffraction peak of pristine GO shows serious restacking phenomenon of GO nanosheets than than that of freeze-drying GO. The diffraction peak appears smaller angle of freeze-drying GO implies the increased interlayer distance after the vaccum freeze-drying process. The possible reasons might be that ice crystals were stuffed into the interspacing of GO sheets to increase the interlayer distance in the process of GO solution was frozen. When the ice crystal was sublimated under high vacuum in the freeze-drying process, the increased interlayer distance was retained.[53] For rGO, it was found a typical (002) diffraction peak position at 26 ° (inset in Fig. S3b). Both GN-f and GN-p show diffraction peaks at 2θ degrees of 37.2, 43.2, 62.7, 75.4, and 79.2 · , which can be indexed as (111), (200), (220), (311), and (222) crystal planes of NiO phase (JCPDS 4-0835), respectively. The peaks of GO in the two samples were disappeared illustrating that the GO was reduced to graphene during the hydrothermal process and calcinations.

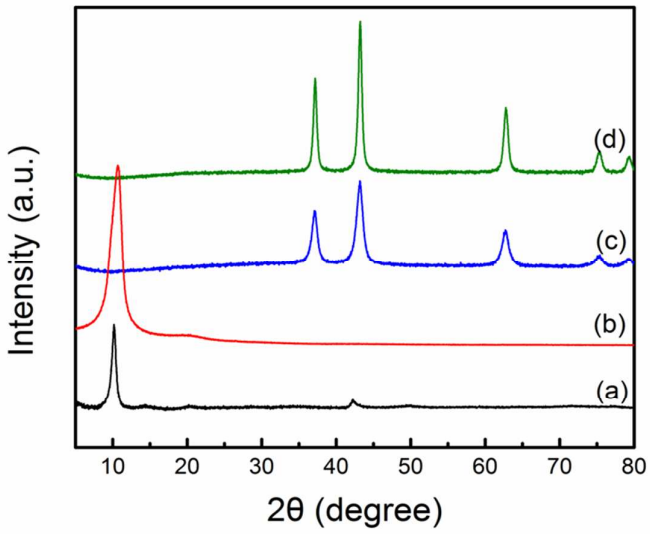

Fig. 2. XRD patterns of freeze-drying GO (a), pristine GO (b), GN-f (c), and GN-p (d)

The FTIR spectra of GO, GN-f, and GN-p are shown in Fig. 3. The spectrum of the oxygen-containing functional groups of GO reveals absorption at 1051, 1224, 1403, and 1739 cm^{-1}, which correspond to the stretching vibrations of alkoxy C–O, epoxy C-O, carboxy C-OH, and C=O groups from carbonyl, and carboxylic groups respectively. The C-O and C=O stretches of rGO were found almost indistinguishable (Fig.S3b). The peak at 1624 cm^{-1} can be assign to bending vibrations of O-H in the adsorbed water molecules and also the contributions from the skeletal vibrations of unoxidized graphitic domains. Compared with GO, these absorption peaks are dramatically weaken in the spectra of GN-f and GN-p composites, suggests that most of the oxygen-containing groups have been removed. The FTIR spectra of GN-f and GN-p exhibit a strong absorption peaks at around 428.8 cm^{-1} corresponding to the Ni-O stretching vibrations of NiO.[54]

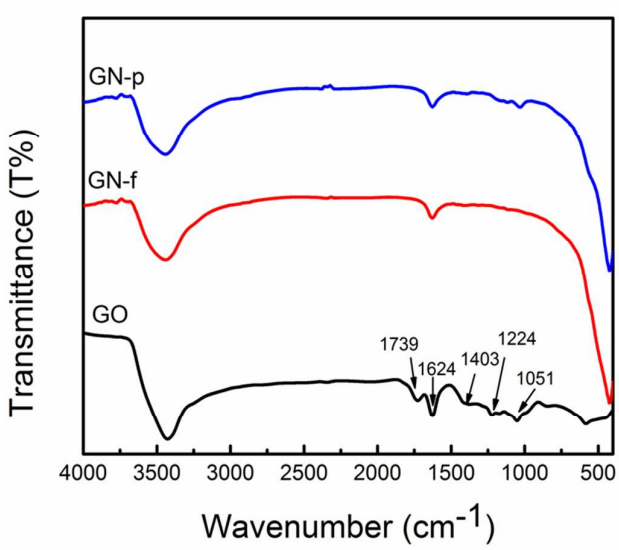

Fig. 3. FTIR spectra of GO, GN-f and GN-p

The surface chemical compositions were further investigated by XPS. In Fig. 4a, the C1s and O1s can be seen in the XPS spectrum of GO. After combination with NiO, two new peaks of Ni $2p_{3/2}$ and Ni $2p_{1/2}$ are appeared, indicating the presence of NiO in the nanocomposites. The Ni 2p peak shows two edge splits by spin-orbital coupling (Fig. 4b), a main peak of $2p_{3/2}$ at 851.1-869.4 eV and a satellite peak of $2p_{1/2}$ at 870-885 eV.[55] Fig. 4c shows the C1s XPS spectra of GO, GN-f and GN-p, which are divided four Gaussian peaks at ~284.8, 286.7, 287.5, and 288.8 eV assigned to C-C/C=C, C-O, C=O, and O=C-O species, respectively. The peaks for C-O, C=O, and O=C-O of rGO declined significantly (Fig. S3a). In contrast with GO, the intensities of three Gaussians peaks for oxygen-containing functional groups become very weak obviously in the C1s XPS spectra of GN-f and GN-p, which indicates most oxygen-containing groups have been removed successfully. Fig. 4d shows the O 1s spectra of GO, GN-f, and GN-p, which can be divided into four peaks. In general, the peak at 529.3 eV correspond to oxygen of NiO.[56] The peak at 531.2 eV is assigned to C=O groups or shoulder peak of O1s of NiO, and the peak at 533.1 eV is ascribed to C-OH and/or C-O-C groups (hydroxyl and/or epoxy). Moreover, compared with the peak located at 533.4 eV in O 1s spectrum of the pristine GO, the content of C-OH

and/or C-O-C groups in the composite is dramatically smaller, which suggests the replacement of hydrogen in hydroxyl groups or a possible ring opening reaction of epoxy groups after the join of Ni^{2+} resulting in the formation of the C-O-Ni linkage.[57] The extra peak located at 530.2 eV is attributed to the possible formation of a C-O-Ni bond.[58]

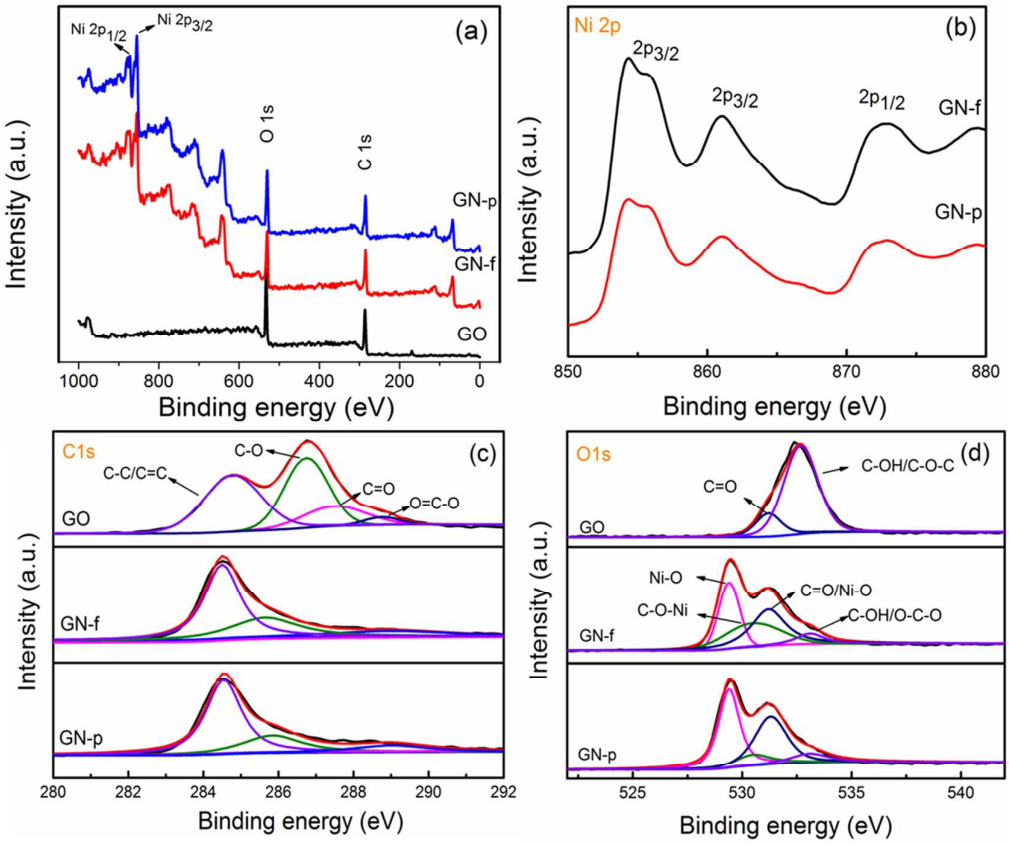

Fig. 4. XPS spectra of (a) survy scan of GO, GN-f, and GN-p, (b) Ni 2p of GN-f, GN-p , (c) C1s, and (d) O1s of GO, GN-f, and GN-p

The thermal properties and composition of NiO/graphene nanocomposites were investigated by TG analysis, which were performed with a heating rate 10 ˚C/min in air atmosphere. As shown in Fig. 5, with the temperature is increased from room temperature to 100 ˚C, the NiO/graphene composites show a slow mass loss, which is due to the loss of adsorbed water molecular. A large mass loss between 250 ˚C and 400 ˚C can be attributed to the removal of graphene from the composites.[59] After 400

℃，the TG curves become stable without further mass loss, indicating graphene removal from the composites completely. The residual wt.-% refers to the weight percentage content of NiO in the composite because it does not lose weight in this experimental condition. The NiO mass ratio of GN-f and GN-p based on TG curves was about 52% and 56%, respectively.

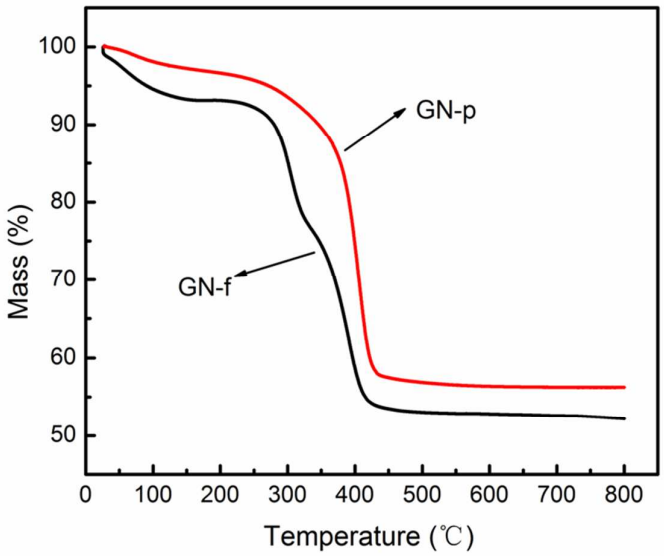

Fig. 5. TG curves of the GN-f and GN-p

Fig. 6 shows the EIS results of GN-f and GN-p. The Nyquist plots of the electrodes are constituted by a single depressed semicircle in the high-medium frequency region and an inclined line at low frequency. The high-medium frequency semicircle is attributed to the charge-transfer impedance on the electrode/electrolyte interface, and the inclined line in the low frequency region corresponds to the ion diffusion process within the electrodes. It is well known that a larger semicircle means a larger charge-transfer resistance and a steeper slope signifies a lower ion-diffusion rate.[60] Obviously, the GN-f exhibits a steeper slope and smaller semicircle than GN-p. It means that the GN-f has a lower ion diffusion resistance and charge transfer resistance. The inset was equivalent circuit, R_e is the solution resistance, C_{dl} is the double layer capacitance, C_p is pseudocapacitance, R_{ct} is the interfacial charge transfer

resistance and Ws is the Warburg impedance due to the distributed resistance within the electrodes. The calculated values of ESR (equivalent series resistance, R_s+R_{ct}) are 1.33 and 1.98 Ω for GN-f and GN-P, respectively.

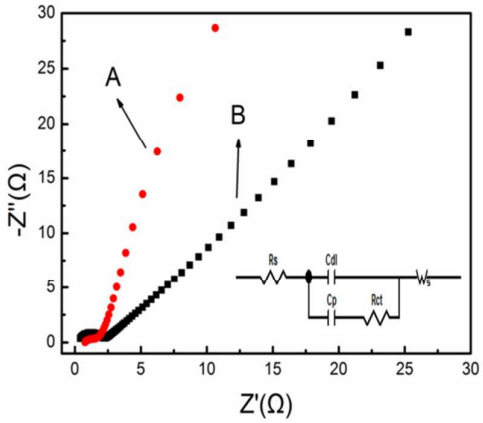

Fig. 6. EIS results of GN-f (A) and GN-p (B), inset is equivalent circuit

The cyclic voltammogram (CV) and galvanostatic charge/discharge (GCD) measurements were operated to study the electrochemical properties of rGO, pure NiO, GN-f and GN-p composites. Fig. 7a show the CV curves rGO, pure NiO, GN-f and GN-p at a scan rate of 50 mV/s with potential windows between 0 V and 0.6 V. It is apparent a pair of redox peaks was observed in all CV curves except for rGO because faradaic reactions happened on NiO, GN-f, and GN-p, which induced to high pseudo-capacitance. The CV curve of pure NiO is narrower than that of the NiO/graphene composites at the same scan rate and indicates the smaller specific capacitances. It can be interpreted that the introduction of GNS increases the capacitance value mainly through improving the conductivity of the NiO. The enclosed area under the CV curve of GN-f is larger than that of GN-p, implying GN-f possesses better capacitive property than that of GN-p, which can be also confirmed in the charge/discharge measurement. In the Fig. 7b, the GCD curves of rGO, pure NiO, GN-f and GN-p composites are carried out at a current density of 1 A/g. The calculated specific capacitance were 387.2, 232.1, 125, and 54 F/g corresponding to GN-f, GN-p, NiO, and rGO, respectively, illustrating the significantly enhanced

capacitance is probably attributed to the recombination of NiO and graphene.[61, 62] On the other hand, GN-f showing better capacitance performance of GN-f than GN-p might be due to that the specific surface areas of GN-f (196.5 m^2/g) was much larger than that of GN-p (124.2 m^2/g). The larger specific area is beneficial to improve the specific capacitance by shortening the diffusion and migration length of the electrolyte ions. In addition, the 3D flowerlike morphology of NiO is favorable to the occurrence of pseudocapcacitance of NiO resulting in an improved specific capacitance of the composite because of its short diffusion path lengths for both electrolyte ions and electrons, favoring the diffusion and migration of electrolyte ions during the rapid charge/discharge process and consequently improving the effective electrochemical utilization of NiO.[37] Furthermore, the lower resistance of GN-f is favorable for enhancing capacitive properties too. Though a lower NiO content in GN-f than that in GN-p, GN-f shows a better capacitance performance than that of GN-p. In the following studies, GN-f was taken as an example for the study of the application to the supercapacitors.

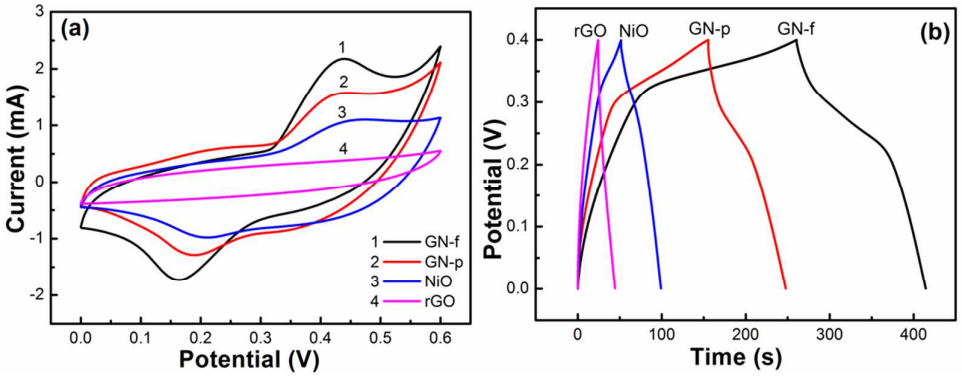

Fig. 7. CV curves at 50 mV/s (a) and galvanostatic charge/discharge curves at 1 A/g (b) of rGO, NiO, GN-p, and GN-f.

The CV curves of GN-f were investigated in the potential window of 0-0.6 V at scan rates of 5, 10, 25, 50, 75, 100, 125, and 150 mV/s in 1M KOH aqueous solution (Fig. 8a). They show similar rectangle-shaped and symmetric shape with a pair of redox peaks, which is attributed to quasireversible redox processes occurring on the surface

of flowerlike NiO microstructure, as shown in eqn3.[63] It indicates this GN-f nanocomposite combined both electrochemical double-layer capacitance and pseudocapacitance.

$$NiO + OH^- \leftrightarrow NiOOH + e^- \qquad (3)$$

The specific capacitances of GN-f at different scan rates are shown in Fig. 8b, the calculated specific capacitance values of GN-f at 5, 10, 25, 50, 75, 100, 125, and 150 mV/s are 500.1, 435.4, 403.9, 339.5, 309.4, 289.8, 263.2, and 246.4 F/g, respectively. Fig. 8c showed the GCD curves of GN-f at different current densities. The calculated specific capacitances of GN-f are 406.2, 402.2, 390, 381, 362 and 326.3 F/g at 0.5, 1.0, 2.0, 3.0, and 5.0 A/g, respectively. It is obvious that the specific capacitance is decreased with the increasing of current density. The high capacitance is attributed to the synergistic effect between graphene that provides the excellent electrical conductivity and NiO that contributes to the high pseudocapacitance. In addition, the unique flowerlike NiO anchored layered graphene sheets, which induced to larger specific surface area of the composite favoring intercalation/extraction of protons into/out of GN-f and shortening the path length for both ions and electrons contributing to the excellent electrochemical performances of GN-f.

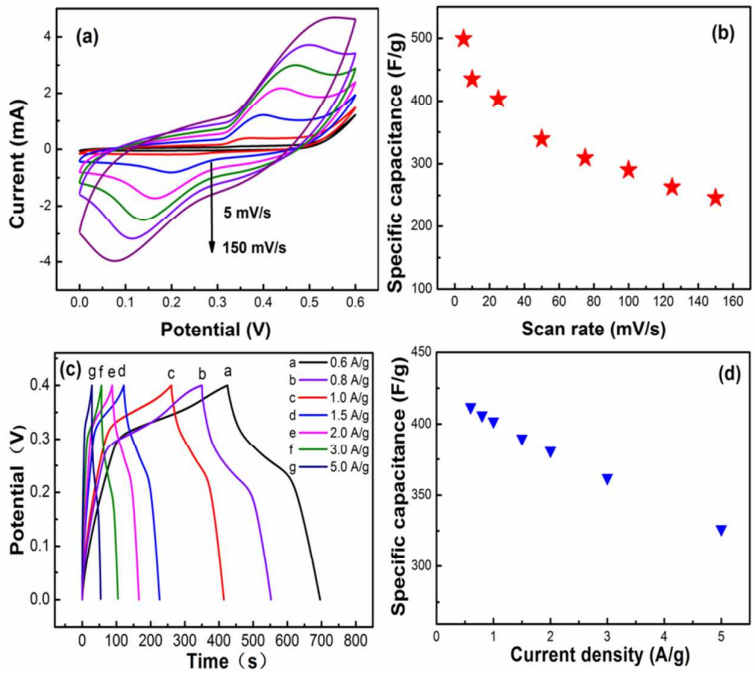

Fig. 8. CV curves of GN-f at different scan rates: from inner to outside (5, 10, 25, 50, 75, 100, 125 and150 mV/s) (a) and the corresponding specific capacitance of GN-f at different scan rates (b). GCD curves of GN-f at different current densities (c) and the corresponding specific capacitance of GN-f (d).

The cycle stability is another important parameter for supercapacitors. The cycle stability of GN-f and GN-p were compared by galvanostatic charge/discharge tested at a current density of 2.0 A/g for 3000 cycles. With the increasing cycles, the specific capacitance of GN-f has a slight decrease until 1000 cycles from 384 to 352 F/g. After that, GN-f showed an obvious decline to 201 F/g while GN-p kept a slight drop between 215 and 181 F/g. As a result, the specific capacitance of GN-p remained 84% of the initial value, which is higher than GN-f (53%). The cycle life test demonstrated polyhydrol NiO/ graphene has better long-term cycle stability than flowerlike NiO/ graphene. The main reason could be assigned to structural instability of GN-f with large size flowerlike NiO adhering to graphene sheets. The porous NiO flowers improved effectively the contact between the active material and the electrolyte and made full use of the active material, while the structure of GN-f could not be preserved long and degraded during the continuous galvanostatic charge/discharge tests. In comparison, polyhedral NiO showed small size and wrapped by graphene sheets, which kept stabilization and then assured the cycle stability of GN-p during the continuous cycling .[64]

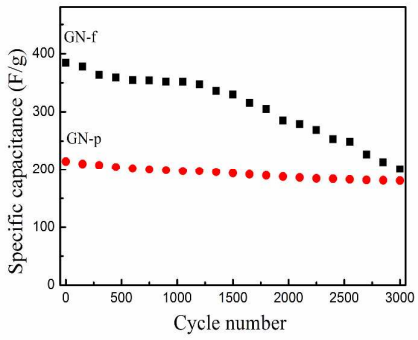

Fig. 9. The specific capacitance changes of GN-f and GN-p at a constant current density of 2.0 A/g as a function of cycle numbers

4. Conclusions

In general, the flowerlike and polyhedral NiO/graphene composites have been successfully synthesized by hydrothermal method, followed by annealing in argon atmosphere. When GO handled with freeze-drying process, the as-prepared composite appears a good-looking flowerlike structure. While the as-prepared GO suspension without freeze-drying process is used, the final corresponding composite present a polyhedral structure. Electrochemical experiments demonstrate that the flowerlike NiO/graphene composite exhibits higher capacitance of 500 F/g at a scan rate of 5 mV/s in 1 M KOH electrolyte but poor long-term cycle life, while the polyhedral NiO/graphene showed a better cycle stability but lower specific capacitance.

Acknowledgments. We sincerely express our thanks to the '973' (2012CB933301) and '863' projects (2011AA050526), the National Natural Science Foundation of China (Nos. 20905038, 20903057, and 61274065), and the Natural Science Foundation of Jiangsu (BK20141424 and BK2011750), and the Priority Academic Program Development of Jiangsu Higher Education Institutions (PAPD), and the Ministry of Education of China (IRT1148).

References

1. G. P. Wang, L. Zhang and J. J. Zhang, *Chem. Soc. Rev.*, 2012, **41**, 797-828.
2. Y. Gogotsi and P. Simon, *Science*, 2011, **334**, 917-918.
3. J. Zhang and X. S. Zhao, *Chem. Sus. Chem*, 2012, **5**, 818-841.
4. E. Raymundo-Pin˜ero, F. Leroux and F. Be´ guin, *Adv. Mater.*, 2006, **18**, 1877-1882.
5. H. Zhang, G. P. Cao and Y. S. Yang, *Energy Environ.Sci.*, 2009, **2**, 932-943.
6. A. M. Osterholm, D. E. Shen, A. L. Dyer and J. R. Reynolds, *Acs. Appl. Mater. Inter.*, 2013, **5**, 13432-13440.
7. G. J. Liu, L. Q. Fan, F. D. Yu, J. H. Wu, L. Liu, Z. Y. Qiu and Q. Liu, *J. Mater.*

Sci., 2013, **48**, 8463-8470.

8. P. Simon and Y. Gogotsi, *Nat. Mater.*, 2008, **7**, 845-854.
9. M. J. Allen, V. C. Tung and R. B. Kaner, *Chem. Rev.*, 2010, **110**, 132-145.
10. N. O. Weiss, H. Zhou, L. Liao, Y. Liu, S. Jiang, Y. Huang and X. Duan, *Adv. Mater.*, 2012, **24**, 5782-5825.
11. K. P. Loh, Q. Bao and P. K. Ang, *J. Mater. Chem.*, 2010, **20**, 2277-2289.
12. Y. Sun, Q. Wu and G. Shi, *Energy Environ. Sci.*, 2011, **4**, 1113-1132.
13. X. An and J. C. Yu, *Rsc Adv.*, 2011, **1**, 1426-1434.
14. S. Bai and X. Shen, *Rsc Adv.*, 2012, **2**, 64-98.
15. J. Wu, W. Pisula and K. Müllen, *Chem. Rev.*, 2007, **107**, 718-747.
16. X. Huang, X. Qi, F. Boey and H. Zhang, *Chem. Soc. Rev.*, 2012, **41**, 525-944.
17. V. Singh, D. Joung, L. Zhai, S. Das, S. I. Khondaker and S. Seal, *Prog. Mater. Sci.*, 2011, **56**, 1178-1271.
18. J. Yan, Z. Fan, W. Sun, G. Ning, T. Wei, Q. Zhang, R. Zhang, L. Zhi and F. Wei, *Adv. Funct. Mater*, 2012, **22**, 2632-2641.
19. G. M. Suppes, B. A. Deore and M. S. Freund, *Langmuir*, 2008, **24**, 1064-1069.
20. B. Wang, J. Park, C. Y. Wang, H. Ahn and A. D. Wang, *Electrochim. Acta,* 2010, **55**, 6812-6817.
21. Y. P. Zhang, H. B. Li, L. K. Pan, Z. S. T. Lu and *J. Electroanal. Chem.*, 2009, **634**, 68-71.
22. S. Chen, J. W. Zhu, X. D. Wu, Q. F. Han and X. Wang, *Acs Nano*, 2010, **4**, 2822-2830.
23. T. Lu, Y. P. Zhang, H. B. Li, L. K. Pan, Y. L. Li and Z. Sun, *Electrochim. Acta*, 2010, **55**, 4170-4173.
24. D. H. Wang, D. W. Choi, J. Li, Z. G. Yang, Z. M. Nie, R. Kou, D. H. Hu, C. M. Wang, L. V. Saraf, J. G. Zhang, I. A. Aksay and J. Liu, *Acs Nano*, 2009, **3**, 907-914.
25. Z. S. Wu, W. C. Ren, L. Wen, L. B. Gao, J. P. Zhao, Z. P. Chen, G. M. Zhou, F. Li and H. M. Cheng, *Acs Nano*, 2010, **4**, 3187-3194.

26. G. M. Zhou, D. W. Wang, F. Li, L. L. Zhang, N. Li, Z. S. Wu, L. Wen, G. Q. Lu and H. M. Cheng, *Chem. Mater.*, 2010, **22**, 5306-5313.
27. K. W. Nam, K. B. Kim and *J. Electrochem. Soc.*, 2002, **149**, 346-354.
28. J. W. Lee, T. Ahn, J. H. Kim, J. M. Ko and J.-D. Kim, *Electrochim Acta*, 2011, **56**, 4849-4857.
29. L. Wang, Y. Hao, Y. Zhao, Q. Lai and X. Xu, *J. Solid State Chem.*, 2010, **183**, 2576-2581.
30. X. J. Zhu, J. Hu, H. L. Dai, L. Ding and L. Jiang, *Electrochim Acta*, 2012, **64**, 23-28.
31. J. Z. e. al., *J. Solid State Chem.,* 2010, **184,** 578-583.
32. L. Kumari, W. Z. Li, C. H. Vannoy, R. M. Leblanc and D. Z. Wang, *Cryst. Res. Technol.*, 2009, **44**, 495-499.
33. J. Zhu, J. Jiang, J. Liu, R. Ding, H. Ding, Y. Feng, G. Wei and X. Huang, *J. Solid State Chem.*, 2011, **184**, 578-583.
34. J. Song, L. Xu, R. Xing, W. Qin, Q. Dai and H. Song, *Sensor Actuat. B- Chem.*, 2013, **182**, 675-681.
35. D. Qiu, Z. Xu, M. Zheng, B. Zhao, L. Pan, L. Pu and Y. Shi, *J. Solid. State Electr.,* 2012, **16**, 1889-1892.
36. D. S. Dalavi, R. S. Devan, R. S. Patil, Y.-R. Ma, M.-G. Kang, J.-H. Kim and P. S. Patil, *J. Mater. Chem. A*, 2013, **1**, 1035-1039
37. C. Ge, F. Zeng, Y. Kuang, Z. Hou, J. Cao, B. He and Y. Liu, *J. Sol-Gel. Sci .Technol.*, 2012, **63**, 146-152.
38. C. C. Li and C. C. Yen, *J. Appl. Electrochem.*, 2008, **38**, 1677-1681.
39. B. Gao, C. Z. Yuan, L. H. Su, S. Y. Chen and X. G. Zhang, Electrochim. Acta, 2009, 54, 3561-3567.
40. W. Xing, F. Li and G. Q. Lu, J. Power Sources, 2004, 134, 324-330.
41. C. Yu, L. Zhang, J. Shi, J. Zhao, J. Gao and D. Yan, Adv. Funct. Mater., 2008, 18, 1544-1554.
42. Y. Jiang, D. Chen, J. Song, Z. Jiao, Q. Ma, H. Zhang, L. Cheng, B. Zhao and Y.

Chu, Electrochimica Acta, 2013, 91, 173-178.

43. B. Zhao, J. Song, P. Liu, W. Xu, T. Fang, Z. Jiao, H. Zhang and Y. Jiang, J. Mater. Chem., 2011, 21, 18792.
44. X. M. Feng, R. M. Li, Y. W. Ma, R. F. Chen, N. E. Shi, Q. L. Fan and W. Huang, *Adv. Funct. Mater.*, 2011, **21**, 2989-2996.
45. J. Zhu and J. He, *ACS Appl. Mater. Interfaces*, 2012, **4**, 1770-1776
46. L. F. Lai, H. P. Yang, L. Wang, B. K. Teh, J. Q. Zhong, H. Chou, L. W. Chen, W. Chen, Z. X. Shen, R. S. Ruoff and J. Y. Lin, *ACS Nano*, 2012, **6**, 5941-5951
47. L. S. Zhong, J. S. Hu, H. P. Liang, A. M. Cao, W. G. Song and L. J. .Wan, *Adv. Mater*, 2006, **18**, 2426-2431.
48. S. Y. Zeng, K. B. Tang, T. W. Li, Z. H. Liang, D. Wang, Y. K. Wang, Y. X. Qi and W. W. Zhou, *J. Phys. Chem. C*, 2008, **112**, 4836-4843.
49. B. Zhao, J. Song, P. Liu, W. Xu, T. Fang, Z. Jiao, H. Zhang and Y. Jiang, *J. Mater. Chem.*, 2011, **21**, 18792-18798.
50. L. S. Zhong, J. S. Hu, H. P. Liang, A. M. Cao, W. G. Song and L. J. Wan, *Adv. Mater.* , 2006, **18**, 2426–2431.
51. S. Y. Zeng, K. B. Tang, T. W. Li, Z. H. Liang, D.Wang, Y. K. Wang, Y. X. Qi and W. W. Zhou, *J. Phys. Chem. C*, 2008, **112**, 4836–4843.
52. G. Huang, S. Xu, S. Lu, L. Li and H. Sun, *Electrochimica Acta*, 2014, **135**, 420-427.
53. D. Cai, S. Wang, L. Ding, P. Lian, S. Zhang, F. Peng and H. Wang, *J. Power Sources*, 2014, **254**, 198-203.
54. Y. Jiang, D. Chen, J. Song, Z. Jiao, Q. Ma, H. Zhang, L. Cheng, B. Zhao and Y. Chu, *Electrochim. Acta*, 2013, **91**, 173-178.
55. B. Varghese, M. V. Reddy, Z. L. Yanwu, C. S., T. C. Hoong, G. V. S. Rao, B. V. R. Chowdari, A. T. S. L. Wee, C. T. and C. H. Sow, *Chem. Mater.*, 2008, **20**, 3360-3367.
56. L. Liu, Y. Li, S. M. Yuan, M. Ge, M. M. Ren, C. S. Sun and Z. J. Zhou, *J. Phys. Chem. C*, 2010, **114**, 251-255.

57. S. Pei, J. zhao, J. Du, W. Ren, H. M. Cheng , Carbon, 2010, **48**, 4466–4474.
58. G. M. Zhou, D. W. Wang, L. C. Yin, N. Li and H. M. Chen, *Acs Nano*, 2012, **6**, 3214-3223.
59. Z. Ji, J. Wu, X. Shen, H. Zhou and H. Xi, *J. Mater. Sci.*, 2010, **46**, 1190-1195.
60. G. F. Cai, J. P. Tu, J. Zhang, Y. J. Mai, Y. Lu, C. D. Gu and X. L. Wang, *Nanoscale*, 2012, **4**, 5724-5730.
61. X. Su, H. Chai, D. Jia, S. Bao, W. Zhou and M. Zhou, *New J. Chem*, 2013, **37**, 439.
62. M. Zhou, H. Chai, D. Jia and W. Zhou, *New J. Chem*, 2014, **38**, 2320.
63. B. Zhao, J. Song, P. Liu, W. Xu, T. Fang, Z. Jiao, H. Zhang and Y. Jiang, *J. Mater. Chem.*, 2011, **21**, 18792-18798.
64. C. Wang, Y. Zhou, M. Y. Ge, X. B. Xu, Z. L. Zhang and J. Z. Jiang, *J. Am. Chem. Soc.*, 2010, **132**, 46–47.

The Synthesis of Shape-Controlled NiO/Graphene Nanocomposites with Enhanced Supercapacitive Properties

Graphical Abstract

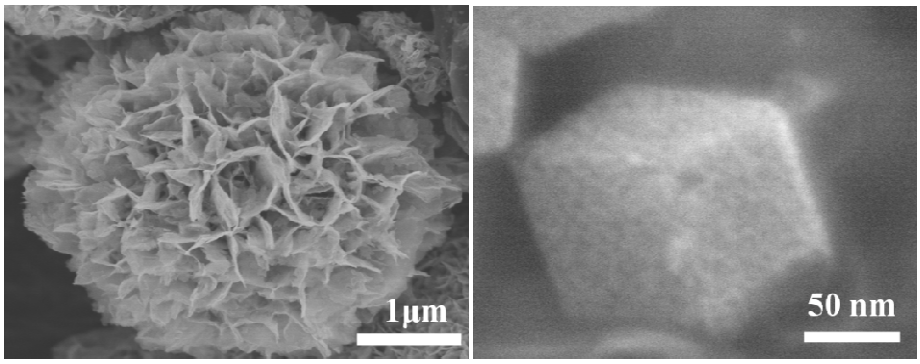

The flowerlike and polyhedral NiO/graphene composites show high supercapacitive performances which were synthesized by a facile hydrothermal method.